

SoLID Project
Solenoidal Large Intensity Device

The SoLID Collaboration

December 6, 2012

1	Contents	
2	List of Figures	ii
3	List of Tables	iii
4	1 Electromagnetic Calorimeter [Draft]	1
5	1.1 Overview	1
6	1.2 Shower Detector	4
7	1.2.1 Sampling Ratio of the Shower Detector	4
8	1.2.2 Total Length of the Calorimeter	5
9	1.2.3 Lateral Size of the Calorimeter Module	5
10	1.3 Preshower Detector	5
11	1.4 Layout and Acceptance	8
12	1.5 Light Readout	8
13	1.6 Radiation Effect	10
14	1.7 Expected Performance	10
15	1.7.1 Electron-pion separation	10
16	1.7.2 Shower Position Measurement	11
17	1.8 Cost Estimation	12
18	1.9 Appendix: PID Selection Cuts	12
19	A Hadron Blind Detectors	15

20 **List of Figures**

21 1 (a) Design diagram of the SoLID electromagnetic calorimeter mod-
 22 (b) a photo of the COMPASS II Shashlyk calorimeter module;
 23 (c) GEANT4 simulation of the shower generated by a 3-GeV
 24 electron incident on the PVDIS calorimeter. The black and green
 25 tracks are secondary photons and electrons respectively. The green
 26 horizontal lines are edges of calorimeter modules. The first two
 27 layers of materials are the preshower detector, consisting of $2X_0$
 28 of lead and 2 cm thick of scintillator. 2

29 2 Energy resolution of the SoLID calorimeter (preshower + shower). 4

30 3 Ratios of energy leak out for an average SIDIS-Forward electron
 31 shower vs. different total length of the calorimeter. 5

32 4 Position resolution and background level from simulation and the
 33 cost of the shower detector vs. lateral block size of the module. . . 6

34 5 Simulated performance for the preshower detector. (a) $1/(\pi^- \text{ Rejection})$
 35 (red curve) at a 95% electron efficiency (blue curve) VS different
 36 thickness of the lead radiator. (b) for a preshower consisting of
 37 $2X_0$ of lead radiator and 2 cm thick of scintillator, left: spectrum
 38 for energy deposition in the scintillator; right: detector efficiency
 39 for different threshold cut. The color code is electron in red, π^- in
 40 blue and μ^- in black. 7

41 6 Reading out photons in the scintillator using a single wavelength
 42 shifting fiber as used in the LHCb experiment [3]. The WLS fiber
 43 is embedded in a circular groove cut by a diamond cutter. 8

44 7 Layout for the SoLID electromagnetic calorimeters: (a) PVDIS
 45 FAEC module layout are in blue and green. SIDIS FAEC module
 46 layout are in blue and red. (b) SIDIS LAEC module layout with
 47 $10 \times 10 \times 60 \text{ cm}^3$ modules in blue, $5 \times 5 \times 41 \text{ cm}^3$ module in green
 48 and $5 \times 5 \times 22 \text{ cm}^3$ module in purple. (c) Side view of SoLID LAEC. 9

49 8 WLS and clear fiber bundle connectors used in the LHCb calorimeter. 10

50 9 Radiation dose rate in each layer of the scintillator tiles in Shashlyk
 51 calorimeter, if there is no preshower. The preshower effectively
 52 block radiation equivalent to the first 20 layers. The color stands
 53 for different contributions of various incoming particles: electrons
 54 (red), photons (blue), EM total (magenta), π^+ (green), π^- (yellow)
 55 and black for total radiation rate. 11

56	10	Overall π^- efficiency (1/rejection) at a constant 94% electron detector efficiency averaged within the acceptance of each calorimeter. For three calorimeter configurations, the track polar angle θ are different, which lead to slight differences in the pion rejection curves.	12
57			
58			
59			
60			
61	11	Position resolution for electrons showers vs. different lateral size of the calorimeter. See text for details.	12
62			
63	12	Illustration of electron sample cuts as highlighted in red dots, in comparison to simulated electron (a) and π^- (b) samples. See text for details.	14
64			
65			

66 **List of Tables**

67	1	Coverage for the SoLID electromagnetic calorimeters. The z direction is along the electron beam and the origin is at the solenoid center. The range of various dimensions are shown.	1
68			
69			
70	2	Summary for the SoLID electromagnetic calorimeters.	3
71	3	Cost estimation for the SoLID calorimeters. There are 1724 large modules (L), which measure $10 \times 10 \times 60 \text{ cm}^3$, and 224 smaller modules (S) with two sizes, $5 \times 5 \times 41 \text{ cm}^3$ and $5 \times 5 \times 22 \text{ cm}^3$.	13
72			
73			

74 1 Electromagnetic Calorimeter [Draft]

75 1.1 Overview

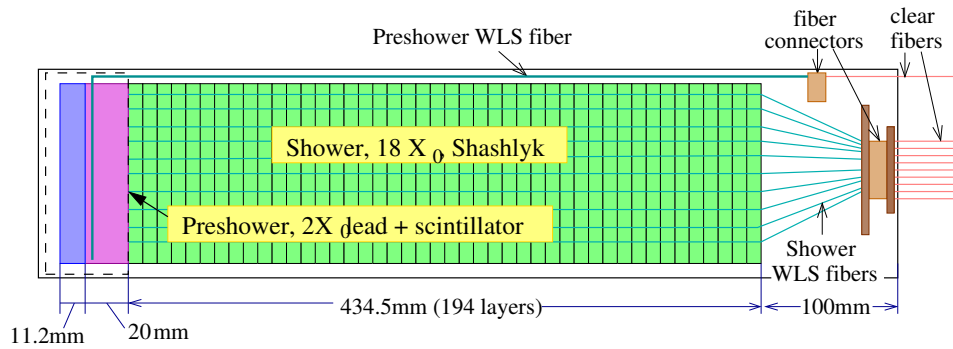
76 Electromagnetic calorimeters (EC) are used in both PVDIS and SIDIS experiments
77 to measure the energy deposition of electrons and hadrons, and to provide particle
78 identification (PID). The incidental hadron is dominated by pions at SoLID energy.
79 There are three calorimeters for the SoLID experiments: the PVDIS experiment
80 uses a forward angle calorimeter (FAEC), and the SIDIS experiments require cov-
81 erages for both a forward angle calorimeter (FAEC) and a large angle calorimeter
(LAEC). The required coverage are summarized in Tab. 1.

	PVDIS FAEC	SIDIS FAEC	SIDIS LAEC
z (cm)	(320, 380)	(405, 465)	(-65, -5)
Polar angle (degree)	(21,36)	(7.5,14.7)	(15.7, 24)
Azimuthal angle	Full coverage		
Radius (cm)	(118, 261)	(100, 220)	(80, 140)
Coverage area (m ²)	17	12	4.5

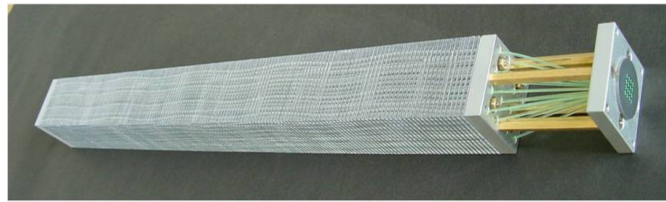
Table 1: Coverage for the SoLID electromagnetic calorimeters. The z direction is along the electron beam and the origin is at the solenoid center. The range of various dimensions are shown.

82
83 The SoLID EC's main characteristics are determined by both the physics goal
84 and the designed running condition of the experiments, as shown in Tab. 2a. The
85 design is challenging due to our unique constraints including high radiation back-
86 ground (~ 500 kRad), strong magnetic field (1.5 T on LAEC) and the budget. These
87 factors prevent the use of many traditional calorimeter technologies, including NaI
88 (TI), CSI, BGO and lead-glass because of their low radiation resistance, PbWO₄,
89 LSO and PbF₂ because of their high cost, and lead/scintillator fiber calorimeter for
90 the high cost and the large amount of light readout required. Two calorimeter tech-
91 nologies that were optimized for the SoLID experiments and met the experimental
92 criteria, were chosen for the shower and the preshower detectors, respectively. As
93 illustrated in Fig. 1a, the shower calorimeter modules are based on the Shashlyk
94 design [1], and the preshower detector consists of a layer of passive radiator fol-
95 lowed by scintillator pads [2, 3]. The overview for these designs are summarized
96 in Tab. 2b and 2c.

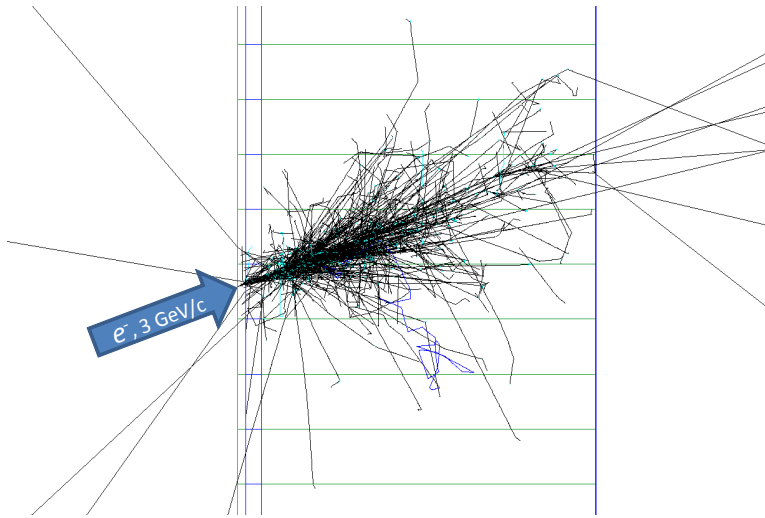
97 A Shashlyk calorimeter is a sampling calorimeter constructed from alternating
98 layers of scintillator and a heavy absorber such as lead. In the experiment, particles
99 incident close to perpendicular to the scintillator-lead layers. Scintillation light is
100 absorbed, re-emitted and transported to the photon detector by wave-length shifting



(a)



(b)



(c)

Figure 1: (a) Design diagram of the SoLID electromagnetic calorimeter module; (b) a photo of the COMPASS II Shashlyk calorimeter module; and (c) GEANT4 simulation of the shower generated by a 3-GeV electron incident on the PVDIS calorimeter. The black and green tracks are secondary photons and electrons respectively. The green horizontal lines are edges of calorimeter modules. The first two layers of materials are the preshower detector, consisting of $2X_0$ of lead and 2 cm thick of scintillator.

	Design specification	Desired performance
π^- rejection	[50-100:1]	\gtrsim [50:1] for above Cerenkov threshold
e^- efficiency	94%	\gtrsim 95%
Energy resolution	$\sim 4\%/\sqrt{E}$	$< 10\%/\sqrt{E}$
Timing resolution	100 ps	< 300 ps
Radiation resistance	500 kRad	\gtrsim 400 kRad
Position resolution	1 cm	\lesssim 1 cm
Longitudinal length	475 cm	-
Lateral granularity	10×10 cm ² , square	-

(a) Overview of the SoLID calorimeter design and desired performance

Type	passive radiator + sensitive layer
passive radiator	$2X_0$, Pb
Sensitive layer	2 cm, plastic scintillator tile
Light transportation	WLS fiber embedded in scintillator

(b) Preshower configuration

Type		Shashlyk sampling calorimeter
Each layer	Absorber	Pb, 0.5 mm
	Scintillator	STYRON 637 plastic scintillator, 1.5 mm
	Gap	Paper, 0.12 mm \times 2 sheets per scintillator layer
	Radiation Length	$9.3 \times 10^{-2} X_0$
Overall	Radiation length (X_0)	24 cm
	Molire radius	5 cm
	Length	$18 X_0$, 43.4 cm
	Layer count	194
	Light transportation	WLS fiber, penetrating layers longitudinally

(c) Shower configuration

Table 2: Summary for the SoLID electromagnetic calorimeters.

101 (WLS) optical fibers penetrating through the calorimeter modules longitudinally
102 along the impact particle direction. Since each 10×10 cm² module contains 100
103 1 mm WLS fibers, the total area required for light readout is reduced by a typical
104 factor of 10^2 compared to the lateral area of the calorimeter.

105 The Institute for High Energy Physics (IHEP) of Russia has extensive experi-
106 ence in the R&D and mass production of Shashlyk type calorimeters. They
107 have successfully developed the Shashlyk calorimeters for many experiments and
108 have been working on building COMPASS calorimeters, as shown in Fig. 1b. Our

109 Shashlyk calorimeter module design is based on the COMPASS module. Geant4-
 110 based simulations, as illustrated in Fig. 1c, was used to study the key specifications
 111 with optimal physics results while minimizing the cost.

112 1.2 Shower Detector

113 1.2.1 Sampling Ratio of the Shower Detector

114 Each layer of the shower module consists of a 1.5 mm-thick scintillator plate and a
 115 0.5-mm absorber plate made of lead. The thickness of the scintillator plate should
 116 be thin enough to ensure fine longitudinal sampling, while thick enough to reduce
 117 light attenuation on the lateral direction. A thickness of 1.5 mm was chosen follow-
 118 ing the experience of previous Shashlyk designs (for the KOPIO experiment [1, 4],
 119 the PANDA experiment [5] and the COMPASS-II experiment as in Fig. 1b). Each
 120 scintillator layer is sandwiched by two sheets of paper which reduce the loss of
 121 scintillation light. Each sheet introduces a gap of $120 \mu\text{m}$ between the lead and
 122 scintillator plates.

123 The Pb absorber thickness of 0.5 mm or less is favored to provide a fine sam-
 124 pling and therefore better energy resolution. With a configuration using 1.5 mm
 125 scintillator and 0.5 mm lead, an energy resolution of about $4\%/\sqrt{E}$ is achieved
 with an effective radiation length of 24 cm, as shown in Fig. 2.

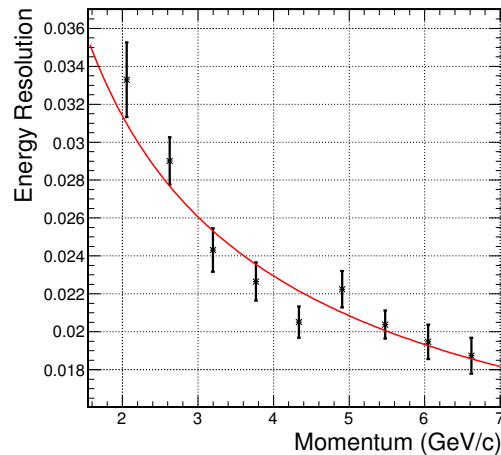


Figure 2: Energy resolution of the SoLID calorimeter (preshower + shower).

126

127 **1.2.2 Total Length of the Calorimeter**

128 The overall length of calorimeter should be long enough to enclose most of the
129 electromagnetic shower and short enough to maximize the difference in energy
130 deposition between electrons and pions. The ratio of energy leak out for elec-
131 tron showers, which were averaged inside the acceptance of the SIDIS-Forward
132 calorimeter, was studied for different total lengths of calorimeter as shown in Fig. 3.
133 A total length of 20 radiation length was found to be a good balance [**Support**
134 **plot**]. Considering a 2 radiation lengths of preshower, this leads to a shower detec-
tor length of 18 radiation lengths or 43.4 cm.

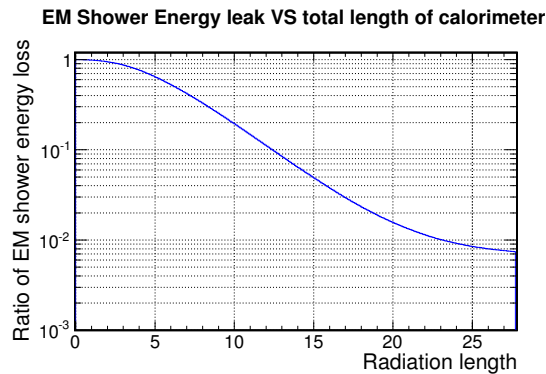


Figure 3: Ratios of energy leak out for an average SIDIS-Forward electron shower vs. different total length of the calorimeter.

135

136 **1.2.3 Lateral Size of the Calorimeter Module**

137 A smaller lateral size for calorimeter modules leads to a better position and lower
138 background; however, this would also increase the total number of modules and
139 channel counts, and therefore higher overall cost. The study shows that a lateral
140 size of about $10 \times 10 \text{ cm}^2$ will provide a good balance between position resolution,
141 background and the overall cost as shown in Fig. 4.

142 **1.3 Preshower Detector**

143 Segmenting the EC longitudinally into a preshower and a shower part is essential to
144 reach the required pion rejection. Several design was considered for the preshower
145 detector, including a full Shashlyk-type design that is optically isolated from the

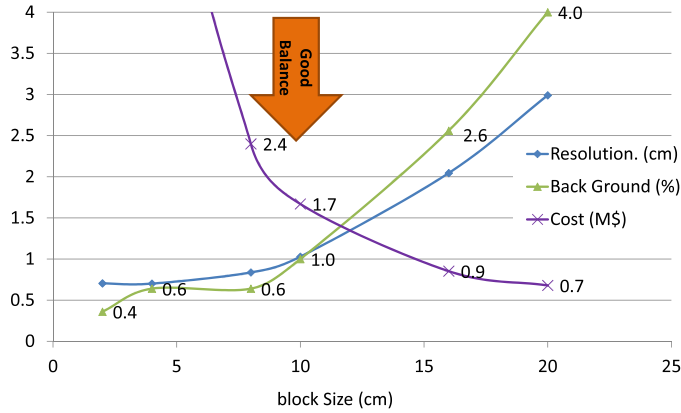
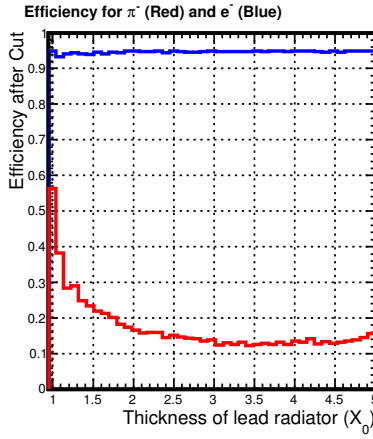


Figure 4: Position resolution and background level from simulation and the cost of the shower detector vs. lateral block size of the module.

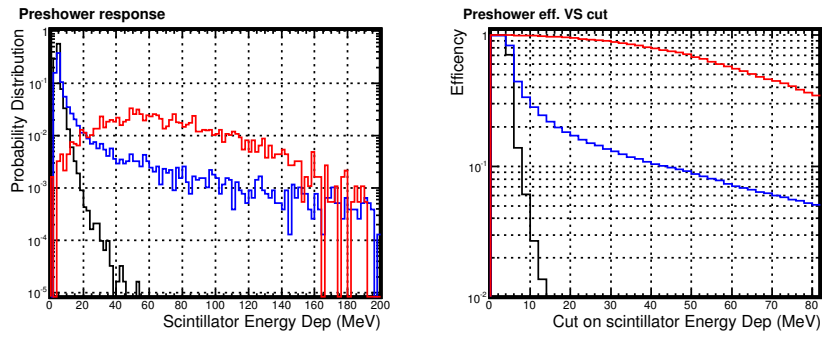
146 shower detector, and a passive radiator/scintillator pad design as used in the HER-
 147 MES [2] and LHCb [3] experiments. Comparing to a Shashlyk-type preshower, the
 148 passive radiator/scintillator pad design have several advantage, including increased
 149 radiation hardness, simplicity in construction and fewer WLS fibers to readout.
 150 For a passive radiator of $2X_0$, the impact to overall energy resolution is less than
 151 $0.5\%/\sqrt{E}$ for electrons with momentum larger than $2 \text{ GeV}/c$. Therefore, the pas-
 152 sive radiator/scintillator pad design was adopted for the preshower detector.

- 153 • The thickness of preshower radiator was determined by optimizing the over-
 154 all pion rejection at the desired electron efficiency. As shown in Fig. 5a, the
 155 preshower-alone pion rejection improves as the radiator thickens up to $3.5X_0$
 156 due to immediate development of the electromagnetic shower. However, the
 157 impact to the overall energy resolution degrades with a thicker absorber. A
 158 radiator thickness of $2X_0$ was found to be the best option for the SoLID
 159 application.
- 160 • The scintillator and readout design is similar to that of the LHCb experi-
 161 ment [3], as illustrated in Fig. 6. A single WLS fiber is embedded in a
 162 2 cm-thick scintillator pad. It absorbs, re-emitted and conducts the photons
 163 for readouts.

164 With the above configuration, the relation between pion rejection and electron effi-
 165 ciency for preshower alone can be plotted as a function of scintillator energy cuts,
 166 as shown in Fig. 5b.



(a)



(b)

Figure 5: Simulated performance for the preshower detector. (a) $1/(\pi^- \text{ Rejection})$ (red curve) at a 95% electron efficiency (blue curve) VS different thickness of the lead radiator. (b) for a preshower consisting of $2X_0$ of lead radiator and 2 cm thick of scintillator, left: spectrum for energy deposition in the scintillator; right: detector efficiency for different threshold cut. The color code is electron in red, π^- in blue and μ^- in black.

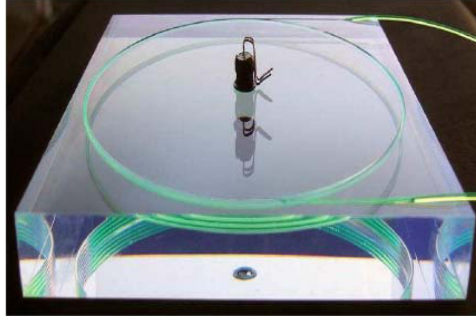


Figure 6: Reading out photons in the scintillator using a single wavelength shifting fiber as used in the LHCb experiment [3]. The WLS fiber is embedded in a circular groove cut by a diamond cutter.

167 **1.4 Layout and Acceptance**

168 The total areas of PVDIS EC and SIDIS ECs coverages are almost the same. The
169 modules will be re-arranged between the two configurations, where modules from
170 PVDIS FAEC will be split and re-arranged into SIDIS FAEC and LAEC. The
171 SIDIS EC layout must preserve the 2-fold rotation symmetry in the spectrometer.
172 The design layout that meets these requirements is shown in Fig. 7.

173 As described earlier, the designed EC modules are about 60-cm long. However,
174 the most inner radius of the SIDIS LAEC cannot use these regular modules because
175 they would block particles and prevent them from reaching the SIDIS FAEC. Mod-
176 ules with a smaller lateral size of $5 \times 5 \text{ cm}^2$ and two shorter lengths (41cm, 22cm)
177 will be used for the inner side of the SIDIS LAEC. The layout for these smaller
178 modules is shown in Fig. 7c.

179 **1.5 Light Readout**

180 The blue light from scintillators is converted into green light by WLS fibers and
181 is carried out to the back of the calorimeters for readout. The Bicon BCF91a
182 WLS fiber is chosen for this project as a balance between the required radiation
183 hardness and the cost. The magnetic field reaches about 1.5 T behind SIDIS LAEC
184 and a few hundred Gauss behind both PVDIS and SIDIS FAEC. Field-insensitive
185 photon sensors are in general expensive and less radiation-hard compared to PMTs.
186 Therefore, the default design is to use clear fibers to further guide the light out of
187 the solenoid for readout by PMTs. The light coupling between WLS and clear
188 fibers can be provided by bundle connectors similar to what LHCb used as shown
189 in Fig. 8.

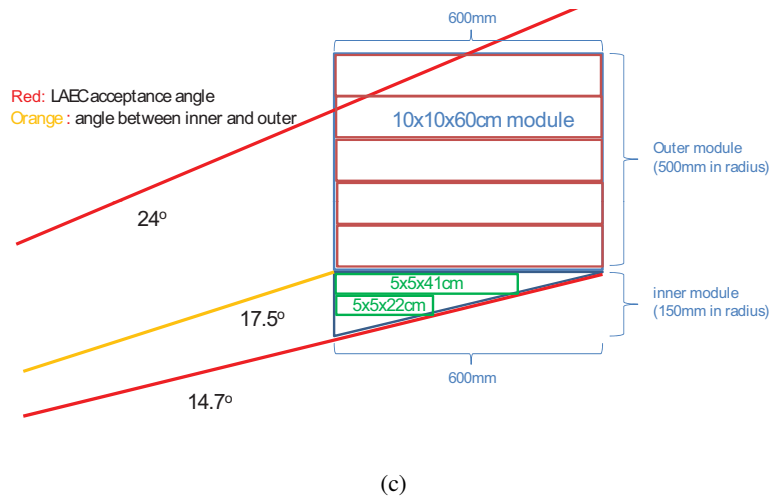
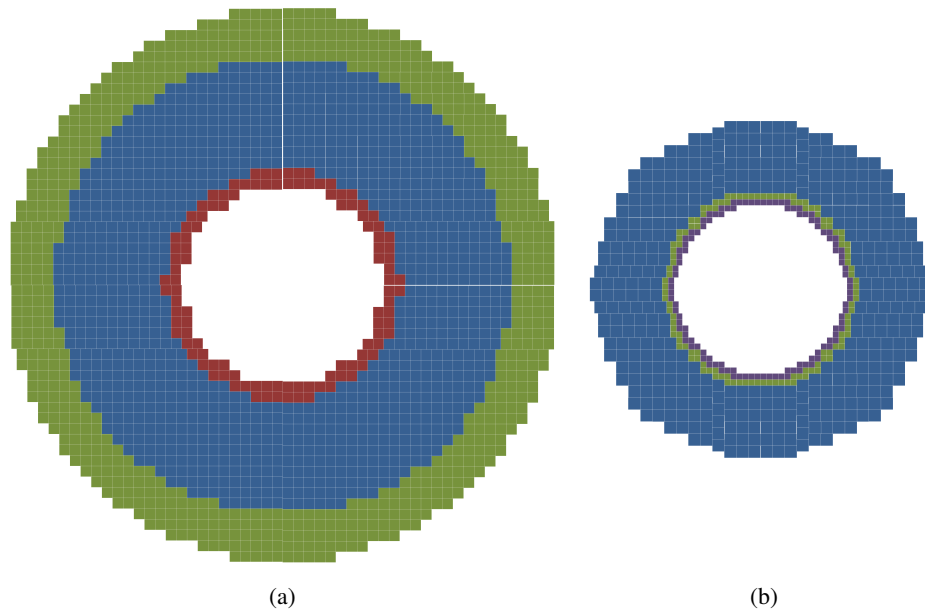


Figure 7: Layout for the SoLID electromagnetic calorimeters: (a) PVDIS FAEC module layout are in blue and green. SIDIS FAEC module layout are in blue and red. (b) SIDIS LAEC module layout with $10 \times 10 \times 60 \text{ cm}^3$ modules in blue, $5 \times 5 \times 41 \text{ cm}^3$ module in green and $5 \times 5 \times 22 \text{ cm}^3$ module in purple. (c) Side view of SoLID LAEC.

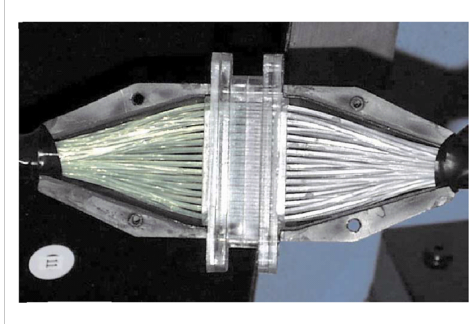


Figure 8: WLS and clear fiber bundle connectors used in the LHCb calorimeter.

190 There are field insensitive photon sensors that can be used for readout. SiPM
191 has enough gain (10^6) for sampling calorimeters, but its dark rate is prone to neu-
192 tron background. We are still evaluating the neutron background at the calorimeters
193 and the choice of SiPM as direct readout without the need of fiber connectors and
194 clear fibers.

195 **1.6 Radiation Effect**

196 The expected luminosities and run time are 169 PAC-days in the PVDIS config-
197 uration at $10^{39} N \cdot \text{cm}^{-2} \text{s}^{-1}$, 245 PAC-days for the SIDIS experiments and 60
198 PAC-days¹ for the J/Ψ experiment at $10^{37} N \cdot \text{cm}^{-2} \text{s}^{-1}$. The radiation level at
199 EC reaches 60 kRad/PAC-year for PVDIS with the baffle and 400 kRad/PAC-year
200 in the SIDIS and J/Ψ experiments, which leads to a total radiation dose of less
201 than 400 kRad for all approved experiments. [TO BE Updated: The COMPASS
202 module has been tested up to 500 kRad. By increasing the thickness of the first few
203 lead layers and using more radiation resistant scintillator and fibers, the radiation
204 hardness can be further improved].

205 **1.7 Expected Performance**

206 **1.7.1 Electron-pion separation**

207 With a multidimensional cut of the preshower and shower response (as shown in
208 Sec. 1.9), the overall pion rejection averaged over the acceptance of each calorime-
209 ter is shown in Fig. 10. For the PVDIS configuration, particles observe longer
210 effective length due to larger incident angles, causing the electromagnetic shower
211 for higher momentum tracks to be contained better inside the calorimeter module.

¹Proposed days, pending PAC beam time assignment.

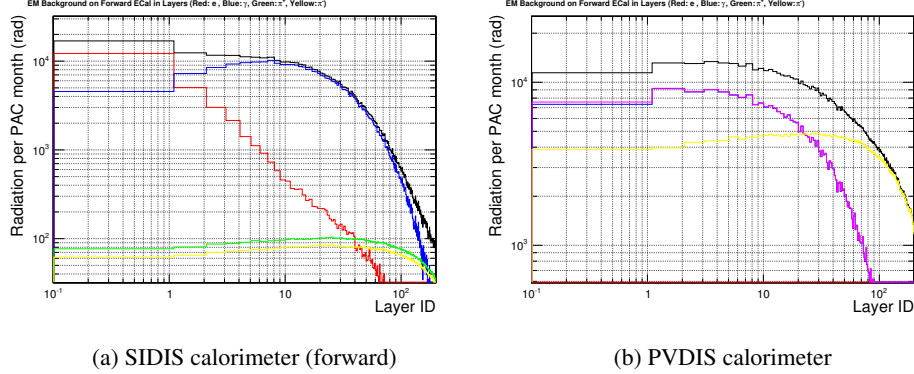


Figure 9: Radiation dose rate in each layer of the scintillator tiles in Shashlyk calorimeter, if there is no preshower. The preshower effectively block radiation equivalent to the first 20 layers. The color stands for different contributions of various incoming particles: electrons (red), photons (blue), EM total (magenta), π^+ (green), π^- (yellow) and black for total radiation rate.

212 The overall π^- rejection with respect to the track momentum P and polar angle θ
 213 can be described as

$$\frac{1}{\pi^- \text{rejection}} \approx 0.01 \left[\frac{3.5 + 0.3 (\theta/\text{degree})}{P / (\text{GeV}/c)} + \frac{1.6 - 0.1 (\theta/\text{degree})}{\sqrt{P / (\text{GeV}/c)}} \right].$$

214

215 1.7.2 Shower Position Measurement

216 The position resolution of the electromagnetic shower center was studied for differ-
 217 ent lateral sizes of the calorimeter modules, as shown in Fig. 11. The red curves are
 218 the position resolutions along the azimuthal direction, for which the tracks are per-
 219 pendicular to the position measurement direction. The blue curves are for the radial
 220 direction for the most extreme incidental angle as in the PVDIS configuration. The
 221 dashed curves are for shower centers calculated using a simple energy-weighted
 222 geometrical center. The solid curves are further corrected with the distribution of
 223 energy deposition between neighboring calorimeter blocks, which flags the full po-
 224 sition resolution for the calorimeter system. At the designed lateral granularity of
 225 $10 \times 10 \text{ cm}^2$, the position resolution is better than 1 cm.

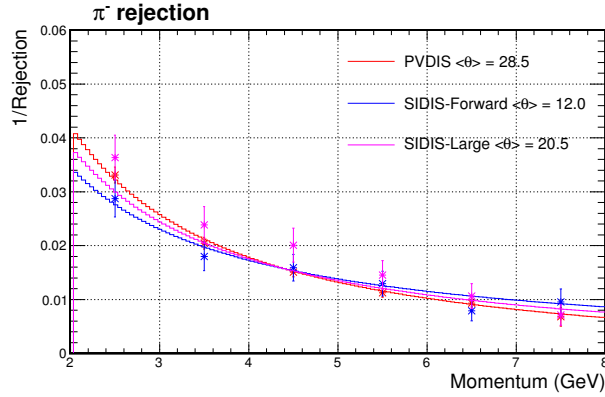


Figure 10: Overall π^- efficiency ($1/\text{rejection}$) at a constant 94% electron detector efficiency averaged within the acceptance of each calorimeter. For three calorimeter configurations, the track polar angle θ are different, which lead to slight differences in the pion rejection curves.

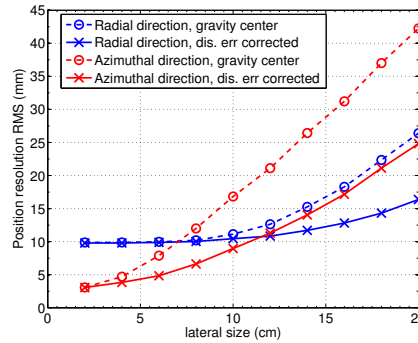


Figure 11: Position resolution for electrons showers vs. different lateral size of the calorimeter. See text for details.

226 1.8 Cost Estimation

227 The estimated cost for the SoLID calorimeters is summarized in Tab. 3. Cost for
228 R&D and prototyping is estimated to be 0.3M\$.

229 1.9 Appendix: PID Selection Cuts

230 A three dimensional PID cut was used to select the best electron samples with
231 maximal π^- rejection as illustrated in Fig. 12. For each given momentum bin, the

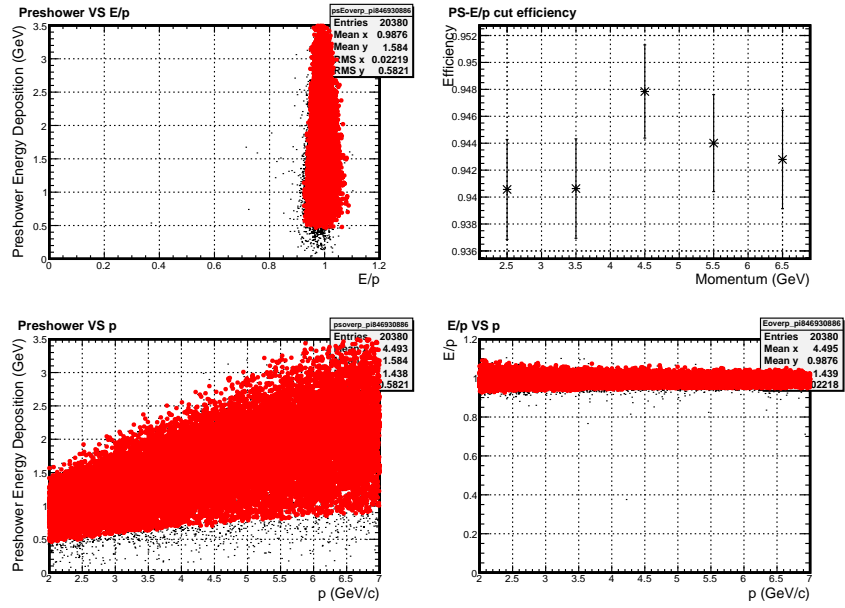
	Per-module cost(\$)	All-module cost(M\$)
Module material	700 (L)/250 (S)	1.26
Module production	800 (L)/500 (S)	1.49
Clear fibers	260 (L)/65 (S)	0.46
Fiber connectors	200	0.39
PMTs	600 x 2	2.34
Labor	5 tech years, 5 student years	0.75
Total	-	6.7
Total+ 30% contingency	-	8.7

Table 3: Cost estimation for the SoLID calorimeters. There are 1724 large modules (L), which measure $10 \times 10 \times 60 \text{ cm}^3$, and 224 smaller modules (S) with two sizes, $5 \times 5 \times 41 \text{ cm}^3$ and $5 \times 5 \times 22 \text{ cm}^3$.

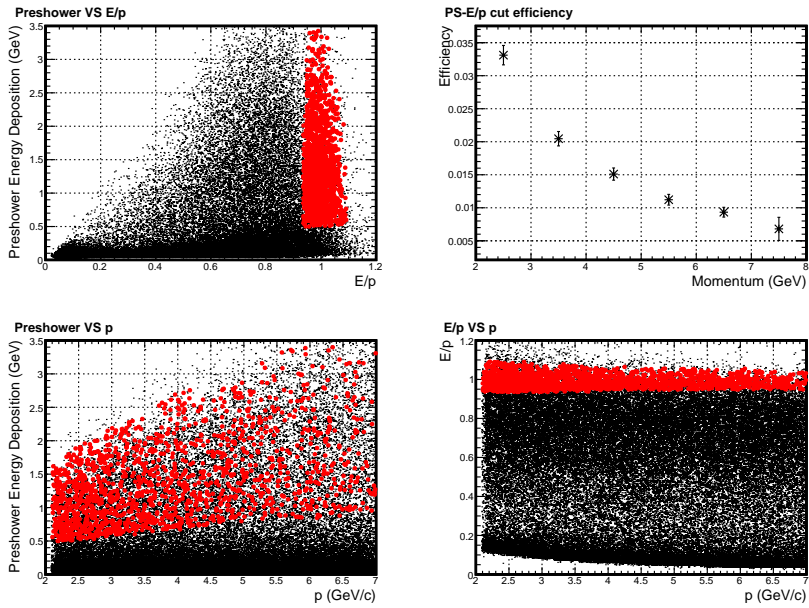
232 cut on E/P and preshower energy roughly follows the contour lines of the ratio
233 of π^- efficiency to e^- efficiency, which is the theoretical best cut for the π^-/e^-
234 separation. A momentum dependence is then introduced to the cut to maintain a
235 constant 94% electron efficiency. Events passing the cut are highlighted in red in
236 the plots.

237 References

- 238 [1] G. Atoian, G. Britvich, S. Chernichenko, S. Dhawan, V. Issakov, et al.,
239 Nucl.Instrum.Meth. **A584**, 291 (2008), 0709.4514.
- 240 [2] H. Avakian, N. Bianchi, G. Capitani, E. De Sanctis, P. Di Nezza, et al.,
241 Nucl.Instrum.Meth. **A417**, 69 (1998), hep-ex/9810004.
- 242 [3] E. P. Olloqui (LHCb Collaboration), J. Phys. Conf. Ser. **160**, 012046 (2009).
- 243 [4] Y. Kharlov et al., Nucl. Instrum. Meth. **A606**, 432 (2009), 0809.3671.
- 244 [5] D. Morozov et al., J. Phys. Conf. Ser. **160**, 012021 (2009).



(a)



(b)

Figure 12: Illustration of electron sample cuts as highlighted in red dots, in comparison to simulated electron (a) and π^- (b) samples. See text for details.

245 **A Hadron Blind Detectors**

246 Your text here [1]

247 **References**

248 [1] Sample citation